

Influence of the spatial and temporal structure of the deposited-energy distribution in swift-ion-induced sputtering

M. Beuve*

Laboratoire d'Informatique Graphique Image et Modelisation, Université Claude Bernard Lyon 1, F-69622 Villeurbanne Cedex, France

N. Stolterfoht

Hahn-Meitner-Institut, Glienickestr. 100, D-14109 Berlin, Germany

M. Toulemonde

CIRIL, Laboratoire CEA-CNRS-ISMRA, BP 5133, F-14070 Caen Cedex 5, France

C. Trautmann

Gesellschaft für Schwerionenforschung, Planckstr. 1, D-64291 Darmstadt, Germany

Herbert M. Urbassek[†]

Fachbereich Physik, Universität Kaiserslautern, Erwin-Schrödinger-Straße, D-67663 Kaiserslautern, Germany

(Received 13 December 2002; revised manuscript received 7 April 2003; published 29 September 2003)

The sputter processes occurring under swift-ion bombardment in the electronic-stopping regime are investigated by molecular-dynamics simulations performed for a Lennard-Jones solid (Ar). Two aspects of the dynamics of the excited electronic subsystem are included in the simulation and their influence on the sputter yield is studied. First, we assume the energy transfer from the electronic to the atomic system not to be instantaneous, but to last for a period of time τ . For $\tau \gg 1$ ps, we find the sputter yield Y to become strongly nonlinear as a function of the stopping power dE/dx . Second, we test the influence of a nonhomogeneous spatial distribution of the electronic excitations. It is shown that such a spatial distribution also leads to a strongly nonlinear dependence of Y on dE/dx .

DOI: 10.1103/PhysRevB.68.125423

PACS number(s): 79.20.Rf, 79.20.Ap, 61.80.Lj

I. INTRODUCTION

When ions bombard a solid target, they may lose energy by collisions with the atomic cores (nuclear stopping) and by creating electronic excitations (electronic stopping). The latter process dominates for ions of energy above a few hundred keV per nucleon (so-called *swift* ions). When penetrating the solid, projectiles of such high energy create a straight cylindrical zone of electronic excitations, the so-called *ion track*. Various processes may lead to severe modifications of the lattice along the ion trajectory.¹ Besides track formation in the bulk, swift ions may also induce sputtering from the surface. The sputter process is quantitatively described by the sputter yield Y , i.e., the number of sputtered particles per incoming ion. Sputter experiments for various systems have shown² that the yield scales with the electronic stopping power dE/dx for certain ranges of velocities as

$$Y \propto (dE/dx)^n. \quad (1)$$

Depending on the material under study, different values were found for the exponent n , e.g., at velocities above the stopping-power maximum: $n=1$ for Ar,^{2,3} $n=2$ for H₂O,⁴ and $n=4$ for LiF.⁵

Several analytical models have been established to describe such a dependence. In some materials, an immediate mechanism of electronic sputtering can be assumed, whereby an individual electronic excitation (such as an exciton) delivers its energy close to the surface, and may induce

sputtering.^{2,6} Such a process obeys a linear sputter law, i.e., $n=1$. Other models have been put up to explain nonlinear sputtering with $n>1$. All of them assume that the electronic excitation energy is converted to the atomic system. In many of these models a *threshold* exists, above which the simple power law [Eq. (1)] holds; the exact value of the threshold stopping power depends on the track radius. For example, the so-called thermal spike models assume that the surface acquires a high energy density which leads to evaporation or sublimation. These models predict $n=2$.^{7,8} In contrast, the so-called pressure-pulse model⁹ assumes that the high pressure building up in the track under the high energy densities delivered there leads to sputtering ($n=3$). The related shockwave model predicts $n=1.5$.¹⁰⁻¹² We note that the exact value of n in these models depends on the details of the assumptions made.

In the last decade, the technique of molecular-dynamics simulation has been used to investigate in detail the processes occurring after a swift ion has penetrated a solid.¹³⁻¹⁹ The molecular-dynamics approach can generally be considered as rather realistic since it is directly suited to simulating nonequilibrium effects in solids. This is in contrast to available continuum models, where the sputter mechanism is based only on surface evaporation. In these molecular-dynamics investigations, above a threshold value of the stopping power, a linear sputter law was found for a fixed track radius, while for smaller stopping powers, in the so-called threshold regime, the exponents n are much larger than 1.¹³ By varying the interatomic potential, the excitation density,

and other parameters, a large number of different simulations^{15,16,18} showed that the linear regime is rather stable and the power exponent only slightly varies around $n=1$. This finding was further confirmed by numerical simulations of the material response and the sputter process based on a hydrodynamic description.^{16,20–22} It also became obvious that a quadratic dependence can only be obtained if the mass transport in the spike is neglected, as it is done in thermal spike models.²⁰ We furthermore note that a recent molecular-dynamics simulation for a condensed O₂ system showed¹⁷ that the power exponent n changes if the size of the track radius is not fixed but increases as a function of dE/dx .¹⁷

In the molecular-dynamics investigations, usually simplified assumptions on the space and time scales of the electron excitation and the energy transfer to the atoms have been employed: The energy is transferred instantaneously to the atoms and is dissipated homogeneously in a cylindrical track volume. To date, there appears to exist only one particular version of the thermal spike model for track formation^{23–25} that includes details of the lateral energy deposition profile and of the time structure of the electron-lattice coupling.^{5,26} Sputter yields obtained with this continuum model exhibit a large nonlinear exponent of $n=4$.⁵

In this paper, we try to find an explanation for the discrepancy between the experimental sputter data exhibiting in many systems $n>1$ and the state-of-the-art molecular-dynamics simulations which typically give $n=1–1.5$. The possible influence of noninstantaneous coupling to the atom system is explored by calculating sputter yields for various rates of energy transfer from the electronic to the atomic subsystem. In addition, we test to what extent the nonhomogeneous energy distribution and also the energy diffusion in the electronic system are of importance.

We perform our molecular-dynamics simulations for the specific case of a Lennard-Jones system, since the evolution of ion tracks has been studied in this system in great detail previously by molecular dynamics, and hence a detailed knowledge already exists.^{13–19} As in these references, we choose the Lennard-Jones parameters to apply for condensed Ar. Note, however, that we do not wish to imply that our results are meant to describe the electronic sputtering of real solid Ar, as here details of the excitation dynamics (excitons) are relevant which are not modeled by us.^{2,3,27} Our simulations should be regarded as a parameter study for a model system designed to test the effects mentioned above.

Two separate aspects of the electron dynamics are treated in this paper: Section III explores the effect of a noninstantaneous energy transfer from the electronic to the atomic system, lasting a coupling time τ . Section IV focusses on the effects of the radial energy deposition profile as it is established by the primary δ electrons, while here a small value of τ is adopted.

II. SYSTEM

In the present paper we use the Ar system for a case study. The atoms interact via the Lennard-Jones potential with a well depth of 10.32 meV and a length parameter of σ

$=3.405 \text{ \AA}$. The system initially has an fcc structure with an atomic density of $n_0=0.025 \text{ \AA}^{-3}$ with (100) surface planes. The sample size was chosen between $30 \times 30 \times 20$ and $80 \times 80 \times 50$ atomic layers. The ion track is situated in the middle part of the square (100) surface plane and runs perpendicular to the surface into the solid; the exact location of the track axis is chosen randomly for each simulation.

The molecular-dynamics code is standard. All surfaces of the model crystal are treated as free surfaces. Atoms are considered sputtered as soon as they become separated from the target atoms by more than the potential cutoff radius, 2.5σ . Due to the symmetry of the ion tracks studied, the sputter yield is taken as the average of forward and backward sputtering. The simulation time is set to between 20 and 70 ps. The time and the sample size are chosen according to the projectile parameters in each case in such a way that (i) the yield saturates with time; (ii) the sample temperature at the lateral simulation boundaries is below half the melting temperature, $T_m=84 \text{ K}$,¹⁵ at the end of the simulation; and (iii) no sputtering could occur from the lateral surfaces due to focusons. The sputter yields given below are averaged over up to 1000 individual ion impacts, in order to get reasonably small error bars. The time step of the velocity-form Verlet algorithm is automatically adapted, and varies from between 0.1 and several 10 fs.

In the course of the simulation, an atom may obtain an energy δE from the electronic system. Since δE is not necessarily small with respect to the atomic kinetic energy, we proceed as follows. If \mathbf{v}_i denotes the initial velocity of atom i , its velocity after the energy transfer is $\mathbf{v}_f=\mathbf{v}_i+\mathbf{q}$, where $\mathbf{q}=q\mathbf{\Omega}$. The value of $q=|\mathbf{q}|$ is obtained by using energy conservation, $Mv_f^2/2=Mv_i^2/2+\delta E$, where M is the atom mass. The direction $\mathbf{\Omega}$ is a random vector uniformly distributed over the accessible domain, which is simply a unit sphere for $\delta E>0$ [note that energy transfer processes from the atoms to the electrons ($\delta E<0$) are ignored in this work].

III. NONINSTANTANEOUS ENERGY TRANSFER

In previous molecular-dynamics simulations of electronic sputtering by swift ions,^{13–19} it was assumed that electrons transfer their energy to the atomic system *instantaneously*, such that only the time evolution of the atomic system needed to be simulated. In this section, we wish to relax this assumption, and rather assume that energy transfer from the electronic to the atomic system lasts a finite period of time τ . The gradual energy deposition is implemented as follows. The track is modeled as a cylinder of radius $r_0=2\sigma$, extending perpendicularly to the surface into the solid. The total energy deposited into the electronic system by each single ion is $E_{\text{tot}}=L \cdot (dE/dx)$, where L denotes the depth of our system, and dE/dx the electronic stopping power. Every time interval Δt , each atom that is at time $t<\tau$ inside the track volume receives an energy $\delta E=(\Delta t/\tau)E_{\text{tot}}/N$ according to the coupling mechanism described in Sec. II. Here N is the total number of atoms that are at time t inside the track cylinder. We verified that our results do not depend on the length of the time step Δt , as long as it is small compared to τ .

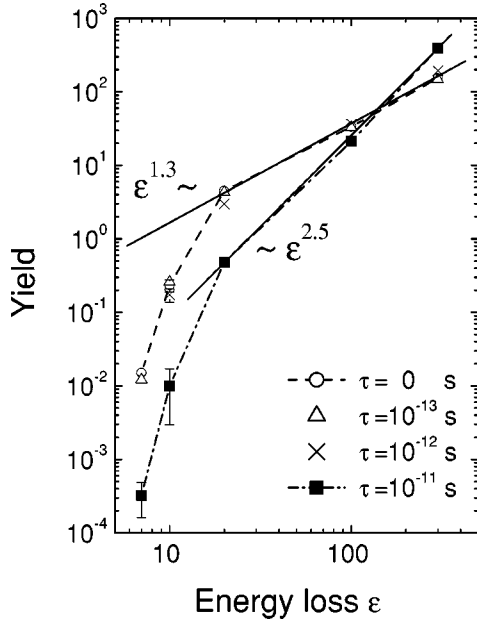


FIG. 1. Sputter yield Y vs scaled energy loss $\epsilon = (dE/dx)(n_0^{1/3}/U)$ for various energy transfer times τ . Error bars denote one standard deviation; if not included, the error bar is smaller than the symbol. The full lines fit the data to a power law, Eq. (1), in the limit of high energy losses ϵ . The dashed lines are included to guide the eye for the $\tau=0$ and the $\tau=10$ ps data.

As is usual for Lennard-Jones systems,¹³ we introduce the scaled energy loss

$$\epsilon = \left(\frac{dE}{dx} \right) / \frac{U}{n_0^{1/3}}, \quad (2)$$

where $U = 80$ meV is the surface binding energy of Ar. Figure 1 shows the dependence of the sputter yield Y on the scaled energy loss ϵ . For a vanishing energy transfer time τ , we recover the results obtained previously for instantaneous energy transfer to the track atoms.^{13,16} Above a critical energy loss $\epsilon_c \cong 20$, sputtering is almost linear with an exponent $n = 1.3$. Here, the sputter yield is $Y(\epsilon_c) \cong 3$, i.e., around one monolayer is sputtered from the track region. Below ϵ_c , the yield quickly decays to zero. For fast transfer times ($\tau = 0.1 - 1$ ps), the yield as a function of the energy loss does not change significantly.

A different behavior appears for larger times, $\tau = 10$ ps. The yield at or below ϵ_c is smaller by almost one order of magnitude than the yield for instantaneous energy transfer. Here, energy flow out of the track volume during the transfer time τ (by heat conduction and by the pressure pulse moving radially out of the cylindrical track) makes less energy available for sputtering and leads to the reduction in yield. Above $\epsilon > \epsilon_c = 20$, the yield data still follow a power law, but the exponent has increased to $n = 2.5$, clearly indicating a nonlinear behavior. For very high energy densities, $\epsilon > 200$, the yield is enhanced by a factor of 2 compared to $\tau = 0$. Here the large amount of energy available in the track close to the surface is used more efficiently for sputtering, since the energy is fueled continuously to the atoms for $\tau = 10$ ps and

less energy is lost by the radial pressure pulse. Note that for smaller values of τ this surplus of energy is not made use of for sputtering.

In a recent simulation²⁸ of Coulomb explosion and its effects on ion tracks it was shown that the sputter yield depends on the *quenching* time τ_{quench} , i.e., on the time required for neutralization. It was demonstrated that the influence of τ_{quench} on the sputter yield levels off only for $\tau_{\text{quench}} \gtrsim \tau_D$, where $\tau_D \cong 0.5$ ps is the Debye period of argon. In our simulation, we observe that the effect of hindered energy transfer from the electronic to the atomic system leads to a nonlinearity in the yield if the energy release time $\tau \gtrsim \tau_D$, namely, for $\tau = 20\tau_D$ (cf. Fig. 1). Since the authors of Ref. 28 also use a homogeneous energy distribution localized in a narrow track cylinder, the results of Ref. 28 and the present simulations appear to be compatible with each other.

IV. INHOMOGENEOUS ELECTRONIC ENERGY DEPOSITION AND TRANSPORT

A. Method

In this section we explore to what extent electronic energy transport processes within the electron subsystem influence the sputter yield. To this end, we describe the electron system via its electronic temperature $T_e(r, t)$ and its dynamics by the heat conduction equation²⁴⁻²⁶

$$C_e \frac{\partial T_e}{\partial t} = \nabla \cdot (\Lambda_e \nabla T_e) - g(T_e - T_a) + A(r, t). \quad (3)$$

The energy deposited into the electronic system is represented by the source term $A(r, t)$. Its space and time dependences are factorized by writing $A(r, t) = F(r)G(t)dE/dx$. Here, dE/dx is the stopping power of the projectile as obtained from, e.g., the SRIM (Refs. 29 and 30) code. $F(r)$ and $G(t)$ are normalized functions characterizing respectively, the space and time dependences of the electronic excitations. $G(t)$ is given by a normalized Gaussian that describes the duration of the electron cascade process. Its width and also its maximum are set here to 1 fs. Note that the factorization of the source term $A(r, t)$ is acceptable due to the small time duration relevant for G . The radial distribution $F(r)$ can in principle be obtained from Monte Carlo calculations,^{31,32} where the electron cascade is followed down to the subexcitation level.³¹⁻³³ For reasons of convenience, however, we employ the analytical expression given by Waligorski *et al.*,³³ which is itself based on Monte Carlo results. It takes into account that the energy profile of the ejected electrons depends on the velocity v_p of the projectile ion. At high v_p , the electrons receive large velocities, up to $2v_p$. These fast δ electrons with range r_{max} thus determine the maximum extent of the radial distribution $F(r)$. For $r < r_{\text{max}}$, $F(r)$ depends roughly like $1/r^2$ on the distance r to the track axis; this dependence is only softened very close to the track axis. As a general consequence, at high v_p , the deposited energy is reduced by smearing out to larger track radii.

In Eq. (3), C_e is the specific heat of the electron system. For the case of insulators studied here, it critically depends on the number of electrons transferred to the conduction

band. For our case study, we assume that C_e is independent of time and space and has a value of $C_e = 1 \text{ J/K cm}^3$. For a nondegenerate free electron gas, this corresponds to 2 electrons/atoms transferred to the conduction band.

Λ_e denotes the electronic heat conductivity. Similar to C_e , we use a space and time independent value, $\Lambda_e = 2 \text{ W/K cm}$. This corresponds to a heat diffusivity $D_e = \Lambda_e / C_e = 200 \text{ nm}^2/\text{ps}$.

The electron-phonon coupling constant g is also taken as space- and time-independent with a value $g = 2 \times 10^{14} \text{ W/cm}^3 \text{ K}$. Due to the electronic band gap in insulators, we exclude energy transfer processes from the atomic subsystem back to the electronic subsystem, i.e., $g = 0$ for $T_e < T_a$.

The particular values adopted for C_e and D_e are identical to the input parameters used by Toulemonde *et al.* when performing thermal spike model calculations for insulators.²⁶ Since in this section we want to treat the special effects associated with an inhomogeneous initial distribution of the deposited energy, we select an unrealistically large value for the coupling constant g (about one order of magnitude larger than in Ref. 26). Such a large value of g corresponds to an extremely short coupling time of $\tau = C_e / g = 5 \text{ fs}$. During this time, the heat in the electron system diffuses over a length

$$\lambda = \sqrt{4D_e\tau} = 2 \text{ nm}. \quad (4)$$

This value is small compared to the size of our simulation crystallite; we may thus neglect energy loss processes at the sample borders.

Our hybrid solution scheme for the dynamics of the coupled electronic and atomic sub-systems works as follows. After each molecular-dynamics time step, we calculate the atomic temperature $T_a(r, t)$ as a function of the radial distance r from the track axis from the molecular-dynamics data. These temperatures are input into Eq. (3), which is then solved using a finite-difference scheme with an appropriate electronic time step (at the beginning of the simulation the electronic time step is as small as 10^{-17} s). From the solution of this equation we obtain the electron temperature T_e and the energy transfer density $\Delta E(r) = g \Delta t (T_e - T_a)$. The energy $\Delta E(r) / n_0$ is given to each atom at distance r . For the numerical solution of Eq. (3) and the calculation of T_a , we divide space into discrete cylindrical shells of width $\Delta r = 5 \text{ \AA}$. Then the simulation proceeds with the next molecular-dynamics time step.

B. Results

Figure 2 displays the time evolution of the electron and atom temperatures for a 2.4-MeV He impact on Ar. The profiles shown correspond to the track axis ($r = 0 \text{ nm}$) and to the two radial distances $r = 0.5$ and 1.5 nm . The electronic temperatures reach their maxima very early, at times between 1 fs in the track center up to at most 5 fs for the larger radii. In the center of the track, the large temperature increase is mainly due to the source term $A(r, t)$, which peaks at 1 fs. At larger distances, the peak is smeared out and moves to larger times. Here, energy transfer by electronic heat conduction from the core to larger radii starts to play a role. Due to the

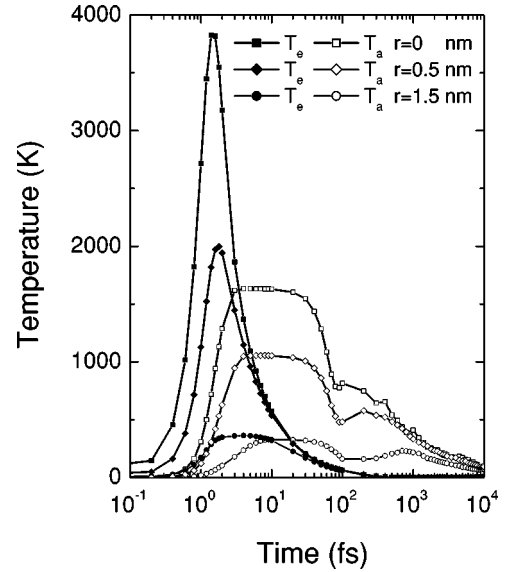


FIG. 2. Electron temperature T_e and atom temperature T_a vs time t at various radial distances r from the track cylinder axis. Data for 0.6-MeV/nucleon He bombardment of Ar, i.e., at the stopping power maximum.

large value of D_e , electronic heat conduction occurs essentially instantaneously on the atomic time scale. As time proceeds, the electronic temperature decays very quickly and becomes negligible beyond 0.1 ps due to rapid electron heat conduction and, in addition, due to the fast electron-phonon coupling time of $\tau = 5 \text{ fs}$ implemented in this model system. As a consequence of this strong coupling, the atom system is quickly energized and reaches its maximum temperature within the first 3–7 fs. For a while (30–50 fs), the atomic temperature remains at a plateau and then decreases, while part of the kinetic energy is transformed into potential energy. At a later time, the atomic temperature reaches a second maximum, which is due to the pressure pulse generated in the hot core of the track. An estimate of the pulse velocity amounts to approximately 20 \AA/ps , this value is close to that obtained in Ref. 13. After about 0.1–1 ps equipartition and equilibrium will be reached.¹⁴

Figure 3 displays the simulated yield data for H and He impacts (see Table I) and compares them with the yields calculated for an energized cylindrical track of radius $r_0 = 2\sigma$ (cf. Fig. 1), which we use as a reference. Drastic differences are observed, which we discuss as follows:

(1) The yields for H and He projectiles show a very steep dependence on the deposited energy. A fit to Eq. (1) gives power exponents of $n = 11$ and 7 for H and He, respectively. This means, in particular, that for small ϵ the yields are by several orders of magnitude smaller than the yield data without inclusion of electron dynamics.

(2) Two reasons contribute to this steep $Y(\epsilon)$ dependence and the correspondingly small yields.

(a) The low sputter yield and its steep dependence on ϵ demonstrate that we are in the *threshold regime*^{13,34} which governs at energy losses below a critical value, $\epsilon < \epsilon_c$, when the energy per atom, E_0 , is only slightly above the sublimation energy U to be overcome for sputtering, $1 \lesssim E_0 / U \lesssim 2$.

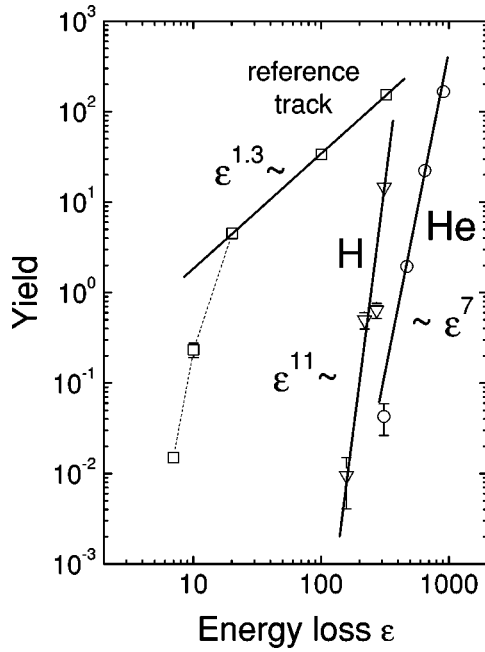


FIG. 3. Sputter yield Y vs scaled energy loss ϵ . Data for H and He bombardment correspond to the energies given in Table I. Data marked “reference track:” simulation without electron dynamics, instantaneous energy transfer to the atoms (cf. Fig. 1, data for $\tau = 0$), included as a reference. Data for H and He: simulation including electron dynamics. Lines: power-law fits [Eq. (1)].

(b) The nonhomogeneous energy deposition profile implies that the electronic excitation is large close to the track axis and small far away. As a consequence, the energy density deposited far from the track axis will be below the threshold value and is hence lost for the sputter process. Also, the energy density close to the track axis will be reduced in comparison to the model case of homogeneous energy deposition. For the case of He impact at maximum stopping power (0.6 MeV/nucleon), the situation close to the track axis is displayed in Fig. 2. Temperatures above the sublimation threshold are reached within a radius of 1.5 nm, i.e., $r_0 = 4\sigma$; this is twice as large as for the reference track. The larger radius and the corresponding lower energy density explain the comparatively small sputter yields of H and He even at the stopping power maximum.

(3) Caution has to be used when comparing the H and He data. The energy deposition profile induced by the electron cascades, i.e., the term $F(r)$ in the energy source term A of Eq. (3), differs for each ion species and energy. In particular, the radial energy density for H and He impact decreases

when the velocity of the projectile increases. This so-called *velocity effect*²³ becomes especially evident if we compare the sputter yields of H and He for the same energy loss, $\epsilon \cong 310$. Here, the velocity of He (6.5 MeV/nucleon) is much higher than that of H (0.11 MeV/nucleon). For He, the energy is therefore deposited farther away from the track axis without contributing to sputtering, resulting in a drastically reduced sputter yield of He (0.04) compared to H (15).

For the impact energies studied here we may thus conclude that the steep $Y(\epsilon)$ dependence can be understood by the joint action of two effects: If the ion velocity increases, ϵ decreases; in addition, this energy is deposited in a larger volume. This combination leads to a huge drop in the energy density and could be responsible for the steep $Y(\epsilon)$ dependence. We note that for the particular case of He and H impact on Ar the existence of the velocity effect has been known for a long time and is well documented, e.g., in the compilation (Fig. 26) of Ref. 2.

V. SUMMARY

In this paper, we investigate the influence of two different features of electron coupling and dynamics. First the effect of a finite electron-atom coupling time τ is studied (Sec. III). Its influence becomes significant as soon as τ becomes large compared to the Debye period of the material.²⁸ At small stopping powers, the yield is reduced because the available energy is distributed over too long a period of time. At large stopping powers, on the other hand, the sputter yield may be even increased, since also the energy contributed late to the atomic system may induce further sputtering. Hence, for not too small energy losses a nonlinear increase of the yield with an exponent of $n = 2.5$, Eq. (1), results.

Second, we model the energy deposition by a realistic non-homogeneous profile (Sec. IV). In this case, a strong decrease of the sputter yield with a high sensitivity on the stopping power—i.e., a high degree of nonlinearity—could be observed. This feature is in part due to the so-called threshold effect, since energy densities—even at the track axis—are not much above the critical value required for sputtering. Furthermore, the velocity dependence of the energy deposition profile is relevant since the energy loss ϵ decreases, when the ion velocity increases above the stopping power maximum; in addition, this energy is deposited in a larger volume.

In summary, we have shown that the inclusion of the spatial and temporal dependence of the deposited energy distribution in the modeling of swift-ion-induced track formation and the ensuing sputtering strongly influences the results. As

TABLE I. Energy E , stopping power dE/dx , and reduced energy loss ϵ for H and He projectiles investigated by molecular-dynamics simulation.

Ion	H	H	H	H ^a	He	He	He	He ^a
E (MeV/nucleon)	0.5	0.3	0.2	0.11	6.5	3.25	1.8	0.6
dE/dx (eV/Å)	3.78	5.23	6.5	7.47	7.42	11.2	15.5	21.7
ϵ	158.5	219	272.5	313	311	470	650	910

^aAt stopping power maximum.

a novel aspect, we included these dependencies in terms of the secondary electrons. In particular, the dependence of the sputter yield on the stopping power may become highly non-linear due to this effect. While the effect of the spatial dependence of the deposited-energy distribution has been included previously via the ion track radius, the inclusion of secondary electrons and their dynamics may prove important for a realistic description of available sputter yield data.

In previous theoretical studies of swift-ion-induced sputtering, the time structure of the energy-deposition process has usually not been taken into account, while the radial

structure has been simplified to a homogeneously excited cylindrical track, and no energy density outside this track. The present paper demonstrates that a relaxation of these simplifying assumptions may sensitively affect the nonlinearity of the sputter yield.

ACKNOWLEDGMENTS

We are grateful to R. E. Johnson and E. Bringa for helpful comments on an early version of the manuscript. M.B. acknowledges financial support by GSI and HMI.

*Also at Hahn-Meitner-Institut, Glienickestr. 100, D-14109 Berlin, Germany; and at Gesellschaft für Schwerionenforschung, Planckstr. 1, D-64291 Darmstadt, Germany

[†]Electronic address: urbassek@rhrk.uni-kl.de; URL: <http://www.physik.uni-kl.de/urbassek/>

¹R. L. Fleischer, P. B. Price, and R. M. Walker, *Nuclear Tracks in Solids* (University of California, Berkeley, 1975).

²R. E. Johnson and J. Schou, *Mat. Fys. Medd. K. Dan. Vidensk. Selsk.* **43**, 403 (1993).

³C. T. Reimann, W. L. Brown, and R. E. Johnson, *Phys. Rev. B* **37**, 1455 (1988).

⁴R. E. Johnson, *Energetic Charged-Particle Interactions with Atmospheres and Surfaces* (Springer, Berlin, 1990).

⁵M. Toulemonde, W. Assmann, C. Trautmann, and F. Grüner, *Phys. Rev. Lett.* **88**, 057602 (2002).

⁶M. Szymanski, *Mat. Fys. Medd. K. Dan. Vidensk. Selsk.* **43**, 495 (1993).

⁷R. E. Johnson and R. Evatt, *Radiat. Eff.* **52**, 187 (1980).

⁸P. Sigmund and C. Claussen, *J. Appl. Phys.* **52**, 990 (1981).

⁹R. E. Johnson, B. U. R. Sundqvist, A. Hedin, and D. Fenyö, *Phys. Rev. B* **40**, 49 (1989).

¹⁰Y. Kitazoe, N. Hiraoka, and Y. Yamamura, *Surf. Sci.* **111**, 381 (1981).

¹¹Y. Yamamura, *Nucl. Instrum. Methods Phys. Res.* **194**, 515 (1982).

¹²I. S. Bitensky and E. S. Parilis, *Nucl. Instrum. Methods Phys. Res. B* **21**, 26 (1987).

¹³H. M. Urbassek, H. Kafemann, and R. E. Johnson, *Phys. Rev. B* **49**, 786 (1994).

¹⁴E. M. Bringa and R. E. Johnson, *Nucl. Instrum. Methods Phys. Res. B* **143**, 513 (1998).

¹⁵E. M. Bringa, R. E. Johnson, and L. Dutkiewicz, *Nucl. Instrum. Methods Phys. Res. B* **152**, 267 (1999).

¹⁶E. M. Bringa, R. E. Johnson, and M. Jakas, *Phys. Rev. B* **60**,

15 107 (1999).

¹⁷E. M. Bringa and R. E. Johnson, *Surf. Sci.* **451**, 108 (2000).

¹⁸E. M. Bringa, M. Jakas, and R. E. Johnson, *Nucl. Instrum. Methods Phys. Res. B* **164–165**, 762 (2000).

¹⁹E. M. Bringa and R. E. Johnson, *Nucl. Instrum. Methods Phys. Res. B* **180**, 99 (2001).

²⁰M. M. Jakas and E. M. Bringa, *Phys. Rev. B* **62**, 824 (2000).

²¹M. M. Jakas, *Radiat. Eff. Defects Solids* **152**, 157 (2000).

²²M. M. Jakas, E. M. Bringa, and R. E. Johnson, *Phys. Rev. B* **65**, 165425 (2002).

²³A. Meftah, F. Brisard, J. M. Costantini, M. Hage-Ali, J. P. Stoquert, F. Studer, and M. Toulemonde, *Phys. Rev. B* **48**, 920 (1993).

²⁴M. Toulemonde, J. M. Costantini, C. Dufour, A. Meftah, E. Paumier, and F. Studer, *Nucl. Instrum. Methods Phys. Res. B* **116**, 37 (1996).

²⁵Z. G. Wang, C. Dufour, E. Paumier, and M. Toulemonde, *J. Phys.: Condens. Matter* **6**, 6733 (1994).

²⁶M. Toulemonde, C. Dufour, A. Meftah, and E. Paumier, *Nucl. Instrum. Methods Phys. Res. B* **166–167**, 903 (2000).

²⁷W. L. Brown, C. T. Reimann, and R. E. Johnson, *Nucl. Instrum. Methods Phys. Res. B* **19/20**, 9 (1987).

²⁸E. M. Bringa and R. E. Johnson, *Phys. Rev. Lett.* **88**, 165501 (2002).

²⁹J. F. Ziegler, J. P. Biersack, and U. Littmark, *The Stopping and Range of Ions in Solids* (Pergamon, New York, 1985).

³⁰J. F. Ziegler, <http://www.srim.org/> (2000).

³¹B. Gervais and S. Bouffard, *Nucl. Instrum. Methods Phys. Res. B* **88**, 355 (1994).

³²M. Beuve, M. Caron, B. Gervais, H. Rothard, A. Clouvas, and C. Potiriadis, *Eur. Phys. J. D* **15**, 293 (2001).

³³M. P. R. Waligorski, R. N. Hamm, and R. Katz, *Nucl. Tracks Radiat. Meas.* **11**, 309 (1986).

³⁴R. E. Johnson, *Int. J. Mass Spectrom. Ion Phys.* **78**, 357 (1987).